Frontiers in Bioscience Landmark

Front. Biosci. (Landmark Ed) **2025**; 30(5): 37393
https://doi.org/10.31083/FBL37393

Original Research

Neutrophil Extracellular Trap Formation Suppressed by Ro 106-9920 Enhances Diabetic Wound Healing by Blocking NLRP3 Inflammasome Activation

Hua Li[1,2,†], Lihua Xu[1,†], Jingying Chen[1], Huijuan Huang[1], Feiteng Liang[3], Shuxiao Li[3], Fuda Huang[1], Junyu Guo[1,2,*]

[1]Department of General Surgery, Affiliated Hospital of Youjiang Medical University for Nationalities, 533000 Baise, Guangxi, China
[2]Key Laboratory of Tumor Molecular Pathology of Baise, 533000 Baise, Guangxi, China
[3]Department of Burns and Plastic Reconstructive Surgery, Affiliated Hospital of Youjiang Medical University for Nationalities, 533000 Baise, Guangxi, China
*Correspondence: guojunyu@ymun.edu.cn (Junyu Guo)
[†]These authors contributed equally.
Academic Editor: Pedro Fonte
Submitted: 24 January 2025 Revised: 18 April 2025 Accepted: 23 April 2025 Published: 19 May 2025

Abstract

Background: The excessive formation of neutrophil extracellular traps (NETs) is involved in delayed wound healing under diabetic conditions. However, potential therapeutic agents remain underexplored. Our present study aimed to explore the effects of Ro 106-9920, a specific nuclear factor kappa B (NF-κB) inhibitor, on diabetic wound healing and to elucidate the underlying mechanisms. **Methods**: A diabetic mouse model was established, and full-thickness wounds were created. Ro 106-9920 was administered, and wound healing was monitored. Protein levels of NET markers and nucleotide-binding oligomerization domain-like receptor protein 3 (NLRP3) inflammasome components were assessed via western blotting and histological analysis. Functional assays were conducted to evaluate the effect of NETs on fibroblasts, endothelial cells, and keratinocytes using conditioned media (CM) from a phorbol 12-myristate 13-acetate (PMA)-treated neutrophil-macrophage coculture model (NET-CM). CM collected from the coculture model after Ro 106-9920 treatment ((NET+Ro 106-9920)-CM) was used to determine its therapeutic potential. **Results**: NET formation and NLRP3 inflammasome activation were significantly elevated in wound tissues of diabetic mice from day 7 ($p < 0.001$). Similar results were observed in PMA-treated neutrophils and macrophages ($p < 0.001$). The viability and migration of endothelial cells, fibroblasts, and keratinocytes, as well as the angiogenic potential of endothelial cells, were significantly impaired by NET-CM treatment (all $p < 0.001$), whereas Ro 106-9920 effectively attenuated these alterations (NET-CM vs. (NET+Ro 106-9920)-CM, cell viability, $p < 0.001$; cell migration, $p < 0.01$; tube formation, $p < 0.001$). *In vivo*, Ro 106-9920 treatment inhibited NET formation, as evidenced by the decreased citrullinated histone H3 (CitH3) and peptidyl arginine deiminase 4 (PAD4) expression ($p < 0.05$). This was followed by a decrease in NLRP3 inflammasome activation ($p < 0.05$), an increase in angiogenesis in wound tissues ($p < 0.001$), and improved wound healing ($p < 0.001$) compared with those in Ro 106-9920-untreated mice. **Conclusions**: Ro 106-9920 enhances diabetic wound healing by suppressing NET formation and inhibiting NLRP3 inflammasome activation, providing a novel therapeutic choice for improving chronic wound healing in patients with diabetes.

Keywords: Ro 106-9920; neutrophil extracellular trap; NLRP3 inflammasome; diabetic wound healing; NF-κB inhibition

1. Introduction

With the global rise in the prevalence of diabetes, the incidence of diabetes-related complications is rapidly increasing [1]. Patients with diabetes are prone to chronic nonhealing wounds, primarily driven by impaired immune responses, persistent inflammation, reduced angiogenesis, and abnormal tissue regeneration. These chronic wounds diminish the quality of life and even increase the risk of infection and mortality, thus imposing a substantial healthcare financial burden [2,3].

Regarding the mechanisms underlying diabetic wound healing and its influencing factors, neutrophil extracellular traps (NETs) are considered key contributors to impaired healing. In response to certain stimuli, such as injury, neutrophils release NETs, web-like structures, through a process called "NETosis". These structures trap pathogens, limiting their spread [4]. However, apart from aiding in pathogen elimination, NETs can also damage the surrounding tissues [4]. In diabetic wound healing, excessive NET formation exacerbates this issue by stimulating immune cells to release proinflammatory mediators or activate certain proinflammatory molecular signals, such as the nucleotide-binding oligomerization domain-like receptor protein 3 (NLRP3) inflammasome. This creates an inflammatory environment that impairs the healing process [5]. Inflammatory responses inhibit the functions of key cells that are closely related to wound healing and disrupt tissue repair, thereby hindering regeneration [6]. A recent

study revealed that miR-26b-5p can target NETs and reduce inflammation in diabetic models, suggesting that inhibiting NET formation may improve wound healing under diabetic conditions. This provides a novel insight for exploring a promising strategy for accelerating wound healing in patients with diabetes [7].

The cellular and molecular mechanisms regulating NET formation are highly complex, with the nuclear factor kappa B (NF-κB) signal playing a potentially essential role in its induction [8,9]. Upon external stimulation, neutrophils activate the NF-κB pathway, allowing NF-κB to translocate to the nucleus, thereby binding to specific genes associated with inflammatory responses and immune regulation. This activation leads to the excessive production of reactive oxygen species (ROS) and proinflammatory factors [10], both of which are essential factors in NET formation. A previous study demonstrated that the protumorigenic effects of NETs are significantly reduced during colorectal cancer liver metastasis, potentially limiting cancer progression [11]. Additionally, excessive ROS can induce NETosis by causing significant DNA damage and activating subsequent DNA repair pathways. The damaged DNA becomes an integral component of the extracellular traps [12].

Ro 106-9920 is a small-molecule inhibitor that specifically blocks the activation of NF-κB by inhibiting ubiquitin ligase, thereby suppressing inflammation and the expression of related genes [13]. Additionally, in a lung cancer study, Ro 106-9920 helped reduce tissue factor expression in A549 cells and alleviated tumor-associated thrombosis [14]. Although Ro 106-9920 has shown promising results in various disease models as an NF-κB inhibitor, its role in diabetic wound healing remains underexplored.

Considering the potential regulatory role of NF-κB inhibitors in NET formation and diabetic wound healing promotion, our study investigated the effects of Ro 106-9920, an NF-κB inhibitor, on wound healing in diabetic mice. By assessing the inhibitory effects of Ro 106-9920 on NET formation, NLRP3 inflammasome activation, and functional improvement in fibroblasts, keratinocytes, and endothelial cells, we evaluated its potential efficacy in accelerating diabetic wound healing.

2. Materials and Methods

2.1 Animal

The Ethics Review Committee of the Affiliated Hospital of Youjiang Medical University for Nationalities approved all of the experiments involving animals (YYFY-LL-2023-084). The study is reported according to the Animal Research: Reporting *In Vivo* Experiments (ARRIVE) guidelines. All processes were conducted strictly complying with the relevant guidelines. Mice were housed in a specific pathogen-free facility at 22 $\pm$ 2 °C and 55 $\pm$ 10% humidity. All mice were exposed to a 12-h light/dark cycle and had ad libitum access to standard chow and water.

2.2 Animal Experimental Schedule

C57BL/6J mice (8–10 weeks old; 17–18 g; male) were provided by the Guangxi Medical University Laboratory Animal Centre (Nanning, China). For diabetes induction, mice were administered a high-fat diet for 4 weeks, followed by an intraperitoneal injection of streptozotocin (STZ; HY-13753, MCE, Monmouth Junction, NJ, USA,50 mg/kg) for five consecutive days [15]. When the fasting blood glucose levels were >300 mg/dL, mice were considered to have been successfully induced with diabetes (DM; n = 21 per group). Mice fed a standard diet were used as controls (Control; n = 9 per group). For the wound healing experiments, a full-thickness excisional wound (8 mm in diameter) was created using a sterile biopsy punch on the dorsal surface of each mouse (Miltex, Inc., York, PA, USA) under anesthesia (1% sodium pentobarbital; P3761, Sigma-Aldrich, Burlington, MA, USA, 50 mg/kg).

To investigate the involvement of NETs in diabetic wound healing, nine control and nine DM mice were used. The wounds were photographed on designated days (1, 3, 7, and 14) after wounding. Mice were euthanized by cervical dislocation on days 3, 7, and 14 after wounding, and the wound tissues were harvested for subsequent analysis.

To explore the potential of Ro 106-9920 in improving wound healing in diabetic mice, DM mice were further divided into two groups, which received dimethyl sulfoxide (DMSO) (DM+vehicle; n = 6 per group) and Ro 106-9920 (5 mg/kg) (MCE, Monmouth Junction, NJ, USA) [16] (DM+Ro 106-9920; n = 6 per group), respectively. The subcutaneous injections were administered at multiple sites around the wounds. At 1, 3, 7, and 14 d after wounding, the blood glucose levels and weight of each mouse were assessed, and the wounds were photographed. The mice were euthanized by cervical dislocation 14 d after wounding for harvesting the wound tissues. All photographed wounds were collected and subsequently analyzed using the ImageJ software (Version number 1.52m, NIH, Bethesda, MD, USA).

2.3 Neutrophil Isolation

Mouse neutrophils were isolated as previously described [17]. The harvested neutrophils were purified using a discontinuous Percoll gradient (62%/81%) and resuspended in RPMI-1640 medium (Gibco, Waltham, MA, USA) for further experiments.

2.4 Neutrophil Purity Estimation

The purity of neutrophil samples was assessed using flow cytometry analysis. The samples were incubated with anti-CD11b (12-0112-82, Thermo Fisher Scientific, Waltham, MA, USA) and anti-Ly6G (11-5931-82, Thermo Fisher Scientific) antibodies for 30 min at 4 °C. Subsequently, cells were washed with phosphate-buffered saline (PBS) and fixed in 2% paraformaldehyde (PFA, HY-Y0333, MCE, Monmouth Junction, NJ, USA) for 15 min at 4 °C.

Finally, cells were washed and resuspended in 150 µL PBS before analysis on a BD FACSCanto II (BD Biosciences, Franklin Lakes, NJ, USA). Data were processed using FlowJo (version 10.4.2; BD Biosciences). Singlets were selected from the Forward Scatter Height (FSC-H) versus Forward Scatter Area (FSC-A) dot plot in the debris exclusion gate (gate 1), while in the singlet gate, CD11b and Ly6G double-positive events were gated to detect neutrophils.

2.5 Cell Treatment and Maintenance

Mouse neutrophils (1×10^6) were seeded in each well of six-well plates with RPMI-1640 medium (Gibco, Waltham, MA, USA). The neutrophils were induced with phorbol 12-myristate 13-acetate (PMA; Sigma-Aldrich, Burlington, MA, USA) at a dose of 100 ng/mL for 3–5 h to trigger NET formation. Mouse RAW264.7 macrophages were obtained from ATCC (TIB-71; Manassas, VA, USA) and seeded at a density of 2×10^5 cells per well into Transwell inserts (0.4 µm pore size; Corning, Corning, NY, USA) containing Dulbecco's Modified Eagle Medium (Gibco). The inserts were placed in the six-well plates containing the neutrophils, with or without PMA treatment, for a 12-h coculture at 37 °C. Following coculturing, the conditioned medium (CM) was collected for subsequent analyses. The CM harvested from the PMA-stimulated coculture system was defined as neutrophil-macrophage coculture model (NET-CM).

To investigate the effect of NET formation on the biological functions of keratinocytes and fibroblasts, cells were treated with NET-CM, whereas controls were treated with CM harvested from the non-PMA-stimulated coculture system.

To determine whether Ro 106-9920 can suppress NET formation (thereby attenuating NET-induced injury of fibroblasts, keratinocytes, and endothelial cells), the PMA-stimulated coculture system was further treated with Ro 106-9920 (2.5 µM) [16], the CM of which was defined as (NET+Ro 106-9920)-CM. Next, mouse fibroblasts (NIH/3T3) (CRL-1658; ATCC), keratinocytes (HaCaT) (T9145; Cell Lines Service, Eppelheim, Germany), and endothelial cells (HUVEC) (PCS-100-010; ATCC) were divided into three groups: control, NET-CM, and (NET+Ro 106-9920)-CM. Cells were treated with NET-CM or (NET+Ro 106-9920)-CM before functional analysis; those treated with CM harvested from the non-PMA-stimulated coculture system were used as the control.

All culture media contained 1% penicillin-streptomycin and 10% fetal bovine serum. All cells were incubated in a humidified incubator at 37 °C and 5% CO_2. All cell lines were validated through negative testing of mycoplasma and STR profiling.

2.6 Immunofluorescence

Mouse neutrophils (1×10^6) were seeded on coverslips before treatment. Treated neutrophils were fixed and permeabilized before being blocked with 5% bovine serum albumin for 1 h. Next, neutrophils were incubated overnight at 4 °C with a primary antibody against citrullinated histone H3 (CitH3; ab281584, Abcam, Cambridge, UK) or NF-κB (AF1234, Beyotime, Shanghai, China). After washing thrice with PBS, the neutrophils were incubated with an Alexa Fluor 488-conjugated secondary antibody (A-11008, 1:1000 dilution; Invitrogen, Waltham, MA, USA) for 1 h at room temperature in the dark. Nuclei were counterstained with 4′,6-diamidino-2-phenylindole (DAPI) for approximately 5 min. Finally, fluorescence images were obtained using a TCS SP8 confocal microscope (Leica Microsystems, Wetzlar, Germany). The mean fluorescence intensity of CitH3 and NF-κB from each group was quantified using FIJI/ImageJ (1.52m, NIH, Bethesda, MD, USA).

2.7 Enzyme-linked Immunosorbent Assay (ELISA)

ELISA was performed to quantify the levels of interleukin (IL)-1β and IL-18 in the supernatants collected from the coculture of neutrophils and RAW264.7 macrophages using the Mouse IL-1β ELISA Kit (PI301, Beyotime) and Mouse IL-18 ELISA Kit (PI553, Beyotime), respectively. To monitor mouse liver and kidney function, the levels of alanine transaminase (ALT), aspartate aminotransferase (AST), serum creatinine (Cre), and blood urea nitrogen (BUN) were assessed using ALT ELISA kit (ELK1921; ELK Biotechnology, Wuhan, China), AST ELISA kit (MBS164085; MyBioSource, San Diego, CA, USA), Creatinine Assay Kit (MBS2611108; MyBioSource), and BUN Assay Kit (MBS2611085; MyBioSource), respectively. Briefly, the diluted supernatants and standards were added to precoated 96-well plates. The absorbance was determined at 450 nm using a microplate reader (BK-9622; BioBASE, Shandong, China). A standard curve was constructed by plotting the absorbance values against the known concentrations of the standards. The resulting regression equation was then used to calculate the unknown sample concentrations from their measured absorbance.

2.8 Cell Viability Assessment

Mouse fibroblasts, keratinocytes, and endothelial cells were seeded into 96-well plates. After overnight cultivation for adherence, the cells were treated with different types of CM. Cell viability was evaluated at 24, 48, and 72 h after treatment using a Cell Counting Kit-8 (CCK-8; Dojindo, Kumamoto, Japan) by measuring the absorbance at 450 nm with a microplate reader (BK-9622, BioBASE).

2.9 Cell Migration Evaluation

Cell migration was assessed using a transwell assay [18]. Treated fibroblasts, keratinocytes, and endothelial cells (5×10^4) were plated in the upper chamber of 8.0

μm pore size transwell inserts (Corning). The lower chamber was filled with normal medium (control), NET-CM, or (NET+Ro 106–9920)-CM. After 24 h of incubation, the migrated cells were fixed and subsequently stained with 0.1% crystal violet solution. The migratory cells were recorded under an inverted microscope (IX-83, Olympus, Tokyo, Japan). For quantification, cells were counted on five random fields per membrane and their numbers were then averaged.

2.10 In Vitro Tube Formation Assay

In vitro tube formation experiments were performed to assess the ability of endothelial cells to form branch points [19]. Endothelial cells (1×10^4) were seeded onto each well of growth factor-reduced Matrigel-coated plates in endothelial basal medium (Lonza, Walkersville, MD, USA) supplemented with normal medium, NET-CM, or (NET+Ro 106–9920)-CM. The cells were cultivated for 6 h, after which images of tube structures were captured under an inverted microscope (Olympus). The number of branch points was defined as the junctions where three or more tubes intersected and was quantified manually using the ImageJ software (NIH).

2.11 Histological Staining

For hematoxylin and eosin (HE) staining, the sections of the collected wound tissues, livers, and kidneys were stained with hematoxylin solution (Sigma-Aldrich) for 5 min, followed by rinsing for 10 min. Next, the hematoxylin-stained sections were differentiated in 1% acidic alcohol for 30 s and then treated with lithium carbonate solution for 1 min to develop the blue color of the nuclei. After rinsing, the sections were further counterstained with eosin solution for 2 min prior to dehydrating, clearing, and mounting. Three random sections per tissue sample were selected, and images of the wound center of each section were captured.

To assess the angiogenesis ability of endothelial cells immunohistochemically, the sections were rehydrated and subjected to antigen retrieval. After blocking with 5% normal goat serum, the sections were incubated with a primary antibody against platelet endothelial cell adhesion molecule-1 (CD31) (ab9498, 1:200 dilution; Abcam) overnight at 4 °C. The next day, the sections were incubated with a horseradish peroxidase (HRP)-conjugated secondary antibody (1:2000 dilution, A0208; Beyotime) for 1 h. The signal was developed using a 3,3′-diaminobenzidine (DAB) substrate kit (Sigma-Aldrich), followed by counterstaining with hematoxylin. Stained sections were dehydrated, cleared, and mounted in a synthetic mounting medium. For this analysis, three random sections from each mouse were selected, and five randomly chosen fields from the images were examined.

Histological stained images were captured under a DM500 light microscope (Leica Microsystems).

2.12 Western Blot Analysis

Wound tissues collected on days 1, 3, 7, and 14 after wounding and cells collected after treatment were lysed to obtain total protein. The protein concentration of each sample was determined using a bicinchoninic acid (BCA) Protein Assay Kit (Thermo Fisher Scientific). Each protein (30 μg) was separated on 10% sodium dodecyl sulfate-polyacrylamide gel electrophoresis (SDS-PAGE) gels and transferred onto polyvinylidene difluoride (PVDF) membranes (Millipore, Burlington, MA, USA). The membranes were blocked with 5% skim milk, followed by overnight incubation at 4 °C with primary antibodies against the following proteins: histone H3 (ab1791, Abcam), CitH3, peptidyl arginine deiminase 4 (PAD4) (LS-C806278-10, LifeSpan BioSciences, Seattle, WA, USA), NLRP3 (AF2155, Beyotime), pro-IL-1β (ab234437, Abcam), IL-1β (ab283818, Abcam), apoptosis-associated speck-like protein containing a caspase recruitment domain (ASC) (AF6234, Beyotime), caspase-1 (AF1681, Beyotime), p-NF-κB (AF5881, Beyotime), and NF-κB. β-actin (AF5003, Beyotime) served as the internal reference. All samples were diluted in 5% skim milk at 1:1000 for use. After washing thrice, the membranes were incubated with an HRP-conjugated secondary antibody (1:5000 dilution, A0208; Beyotime) for 1 h at 25 °C. Protein bands were visualized using an enhanced chemiluminescence detection kit (P0018FS, Beyotime) and imaged using the ChemiDoc MP Imaging System (Bio-Rad, Hercules, CA, USA). Densitometric analysis was performed using the ImageJ software (NIH), with H3 or β-actin serving as the loading controls.

2.13 Statistical Analysis

All data are expressed as the mean $\pm$ standard error of the mean. Statistical analyses were performed using GraphPad Prism software (version 9.0, GraphPad Software, San Diego, CA, USA). Comparisons between two groups were performed using the Student's *t*-test. Comparisons among groups were performed using one- or two-way analysis of variance (ANOVA), followed by Tukey's post hoc test. Statistical significance was set at $p < 0.05$.

3. Results

3.1 NET Formation and NLRP3 Inflammasome Activation is Associated With Delayed Wound Healing in DM

The experimental design and groups are shown in Fig. 1A. We observed the wound healing process for 14 d, and found that it was significantly delayed in the DM group compared with that in the control group (Fig. 1B) ($F(3, 64) = 31.26$, $p < 0.001$). Regarding NET formation markers, we detected a marked increase in CitH3 expression in the DM group from day 7 onward compared with that in the control group ($p < 0.001$). In addition, the PAD4 levels were elevated in the DM group as early as day 3 ($p < 0.01$), suggesting the early initiation of NET formation under diabetic conditions (Fig. 1C). Furthermore, we found

that the NLRP3 inflammasome and IL-1β/pro-IL-1β axis were significantly upregulated in the DM group from days 7 ($p < 0.001$) and 3 ($p < 0.001$), respectively (Fig. 1D). Cleavage of the inactive precursor pro-IL-1β releases the bioactive molecule IL-1β that triggers identical biological responses, such as inflammation [20]. Our results suggested that hyperglycemia can enhance the processing of pro-IL-1β to IL-1β, thereby increasing IL-1β secretion in the lesions. Hence, sustained NET formation and prolonged NLRP3 inflammasome activation may contribute to the delayed wound healing observed in DM.

3.2 NET Formation Hinders Fibroblast and Keratinocyte Function through NLRP3 Inflammasome Activation in Macrophages

Neutrophil identification is shown in **Supplementary Fig. 1**. The isolated neutrophils displayed a uniform shape and spherical structure (**Supplementary Fig. 1A**). Further validation of the purity of the isolated neutrophils is demonstrated in the flow cytometry analysis, where >95% of the cells are positive for both Ly6G and CD11b, indicating a highly specific and pure neutrophil population (**Supplementary Fig. 1B**). To investigate the effects of NETs on skin cell function, we treated purified mouse neutrophils with PMA to induce NET formation (Fig. 2A). After coculturing with RAW264.7 mouse macrophages for 12 h, immunofluorescence and western blot analyses revealed a significant increase in CitH3 expression in PMA-stimulated neutrophils compared with that in the untreated control (Fig. 2B,C; both $p < 0.001$). This finding confirmed the successful induction of NETs. Subsequent ELISA analysis of the coculture supernatant demonstrated a notable elevation in the levels of proinflammatory cytokines IL-1β and IL-18 in the PMA group, which coincided with elevated CitH3 levels (Fig. 2D,E; both $p < 0.001$). Additionally, western blot analyses of macrophages revealed the upregulation of the expression of NLRP3, ASC, and caspase-1 in response to PMA treatment, indicating the activation of the NLRP3 inflammasome (Fig. 2F; all $p < 0.001$).

To further assess the functional effect of NETs on skin cells, including fibroblasts and keratinocytes, we applied CM from the coculture system to these cell types (Fig. 2A). The CCK-8 assay demonstrated a significant reduction in the viability of both fibroblasts and keratinocytes after 24, 48, and 72 h of NET-CM treatment compared with that in cells treated with normal medium (control) (Fig. 2G,H; both $p < 0.001$). Moreover, we observed that the migration rates of fibroblasts ($p < 0.001$) and keratinocytes ($p < 0.01$) were markedly decreased in the presence of CM, suggesting impaired wound-healing capabilities (Fig. 2I,J). To explore the potential involvement of the NF-κB signaling pathway in this process, we conducted further immunofluorescence and western blot analyses. We detected a significant increase in NF-κB expression, as indicated by the elevated fluorescence (Fig. 2K; $p < 0.001$), and protein p-NF-κB/NF-κB levels in neutrophils following PMA treatment (Fig. 2L; $p < 0.01$). Collectively, these findings indicated that NET formation promotes NLRP3 inflammasome activation in macrophages, leading to the secretion of proinflammatory cytokines that impair the proliferation and migration of fibroblasts and keratinocytes. Therefore, we hypothesized that the activation of the NF-κB pathway may be involved in this process.

3.3 Ro 106-9920 Mitigates NET-induced Damage to Fibroblasts and Keratinocytes via Inhibition of the NF-κB Signaling Pathway

We introduced Ro 106-9920 to explore its effect in NET formation. We observed a significant reduction in p-NF-κB protein expression in PMA-induced neutrophils after Ro 106-9920 treatment (NET vs. NET+Ro 106-9920 groups, $p < 0.001$; Fig. 3A). Additionally, Ro 106-9920 treatment reversed the PMA-induced elevated expression of CitH3 (NET vs. NET+Ro 106-9920 groups, $p < 0.001$), effectively inhibiting NET formation (Fig. 3B). This inhibitory effect extended to the secretion of proinflammatory cytokines, as evidenced by the decreased levels of IL-1β ($p < 0.001$) and IL-18 ($p < 0.01$) in the culture supernatant of the NET+Ro 106-9920 group compared with that of the NET group (Fig. 3C,D). Furthermore, we observed that the expression of NLRP3 ($p < 0.01$), ASC ($p < 0.001$), and caspase-1 ($p < 0.001$) was markedly suppressed in macrophages in the NET+Ro 106-9920 group, suggesting that Ro 106-9920 effectively attenuates NET-induced NLRP3 inflammasome activation (Fig. 3E).

Subsequent functional assays revealed that the viability of fibroblasts and keratinocytes was significantly higher in the (NET+Ro 106-9920)-CM group than in the NET-CM group after 72 h (Fig. 3F,G; both $p < 0.001$). Moreover, we found that Ro 106-9920 treatment significantly improved the impaired migratory ability of fibroblasts and keratinocytes in the NET-CM group (Fig. 3H,I; both $p < 0.01$). These findings indicated that suppression of the NF-κB signaling pathway by Ro 106-9920 not only inhibits NET formation but also mitigates the associated inflammatory response, thereby protecting fibroblasts and keratinocytes from NET-induced damage.

3.4 Ro 106-9920 Mitigates NET-induced Endothelial Cell Dysfunction by Inhibiting the NF-κB Pathway

Angiogenesis provides the blood and nutritional supply necessary to support wound tissue repair and regeneration [21]. To investigate whether Ro 106-9920 could mitigate the adverse effects of NETs on the angiogenic capacity of endothelial cells, we applied CM collected from cocultures with or without Ro 106-9920 treatment to endothelial cells for 72 h. Despite a general decline in endothelial cell viability following NET formation, the viability of cells treated with Ro 106-9920-CM was significantly higher than that of cells treated with NET-CM (Fig. 4A; $p < 0.001$). Mi-

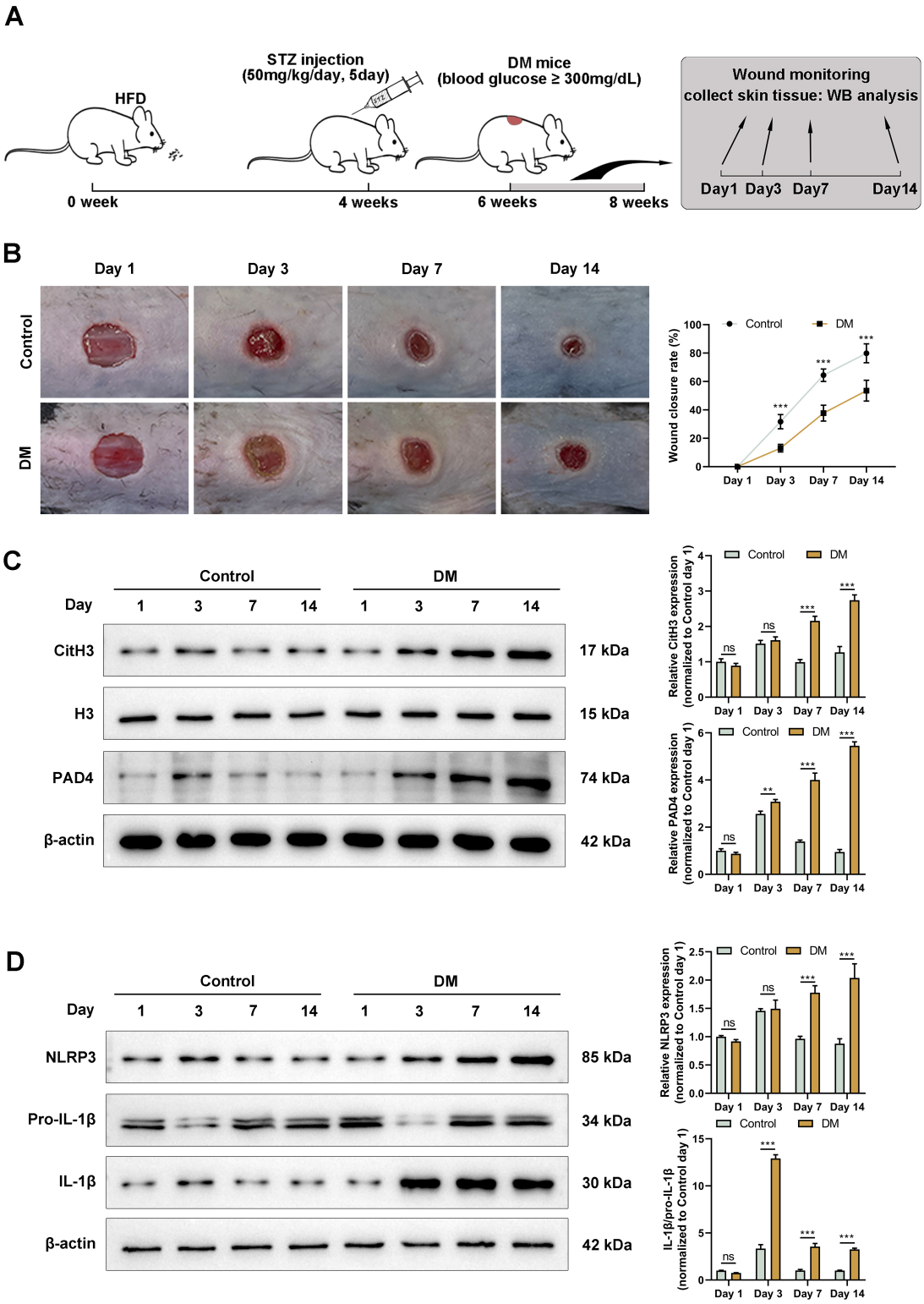

Fig. 1. Sustained neutrophil extracellular trap (NET) formation and nucleotide-binding oligomerization domain-like receptor protein 3 (NLRP3) inflammasome activation in the skin wounds of diabetic mice. (A) After successfully inducing a diabetic mouse model through a high-fat diet combined with streptozotocin injection, an 8-mm full-thickness skin wound was created on the dorsal surface of the mice. (B) Photographs of the dorsal wounds were taken on days 1, 3, 7, and 14 and the changes in wound closure were recorded (n = 3 per group). Western blot analysis was conducted using the wound tissues of mice. (C) Citrullinated histone H3 (CitH3) and peptidyl arginine deiminase 4 (PAD4) expression represented NET formation (n = 3 per group). (D) NLRP3 inflammasome activation was evaluated by assessing the protein levels of NLRP3, pro-interleukin (IL)-1β, and IL-1β (n = 3 per group). ns, no significance, **$p < 0.01$, ***$p < 0.001$. HFD, high fat diet; WB, Western Blot; STZ, streptozotocin; DM, diabetes mice.

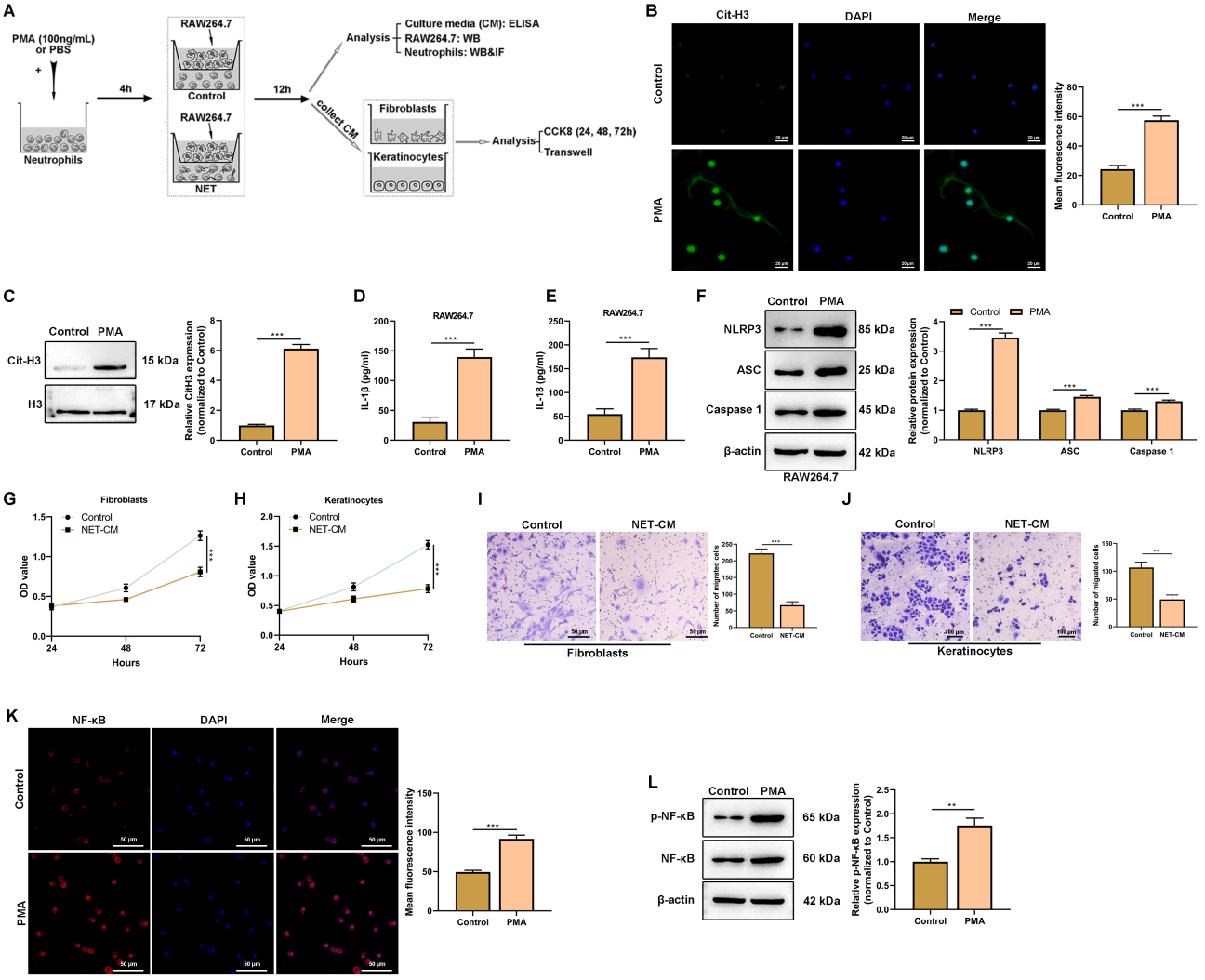

Fig. 2. NETs impair the proliferation and migration of fibroblasts and keratinocytes by inducing NLRP3 inflammasome activation in macrophages. (A) The experimental design and groups of the *in vitro* analysis. Purified mouse neutrophils were treated with phorbol 12-myristate 13-acetate (PMA) to induce NET formation, which was verified by assessing CitH3 expression in (B) immunofluorescence (n = 3 per group, scale bar = 20 μm) and (C) western blot analyses (n = 3 per group). After coculturing with mouse macrophage RAW264.7 cells for 12 h, the supernatant was collected for (D) IL-1β and (E) IL-18 measurement via enzyme-linked immunosorbent assay (ELISA) and used as conditioned media (CM) in subsequent assays (n = 3 per group). (F) Western blot analysis of macrophages cocultured with NET-forming neutrophils revealed the protein levels of NLRP3, apoptosis-associated speck-like protein (ASC), and caspase-1 (n = 3 per group). Fibroblasts and keratinocytes were subsequently treated with CM for 72 h. (G,H) Cell viability at 24, 48, and 72 h after treatment, as demonstrated in Cell Counting Kit-8 (CCK-8) assays (n = 3 per group). After treatment, (I,J) the migration rate of cells was detected using the transwell assay (n = 3 per group). (K) Immunofluorescence (scale bar = 50 μm) and (L) western blot analyses were performed to demonstrate the activation of the nuclear factor kappa B (NF-κB) signal pathway in neutrophils (n = 3 per group) following PMA treatment. $^{**}p < 0.01$, $^{***}p < 0.001$. DAPI, 4′,6-diamidino-2-phenylindole; NET-CM, neutrophil-macrophage coculture model; OD, Optical Density.

gration assays using the transwell system revealed a similar trend. Although NET formation led to a reduced migration rate of endothelial cells, the degree of inhibition was lower in the Ro 106-9920-CM group, indicating that Ro 106-9920 partially restores the NET-induced impairment in endothelial cell migration (Fig. 4B; $p < 0.01$). Moreover, an analysis of angiogenic potential showed that the number of branch points was significantly higher in the (NET + Ro 106-9920)-CM group than that in the NET-CM group (Fig. 4C; $p < 0.001$). These results indicated that Ro 106-9920 confers a protective effect on endothelial cells by mitigating the detrimental effects of NETs.

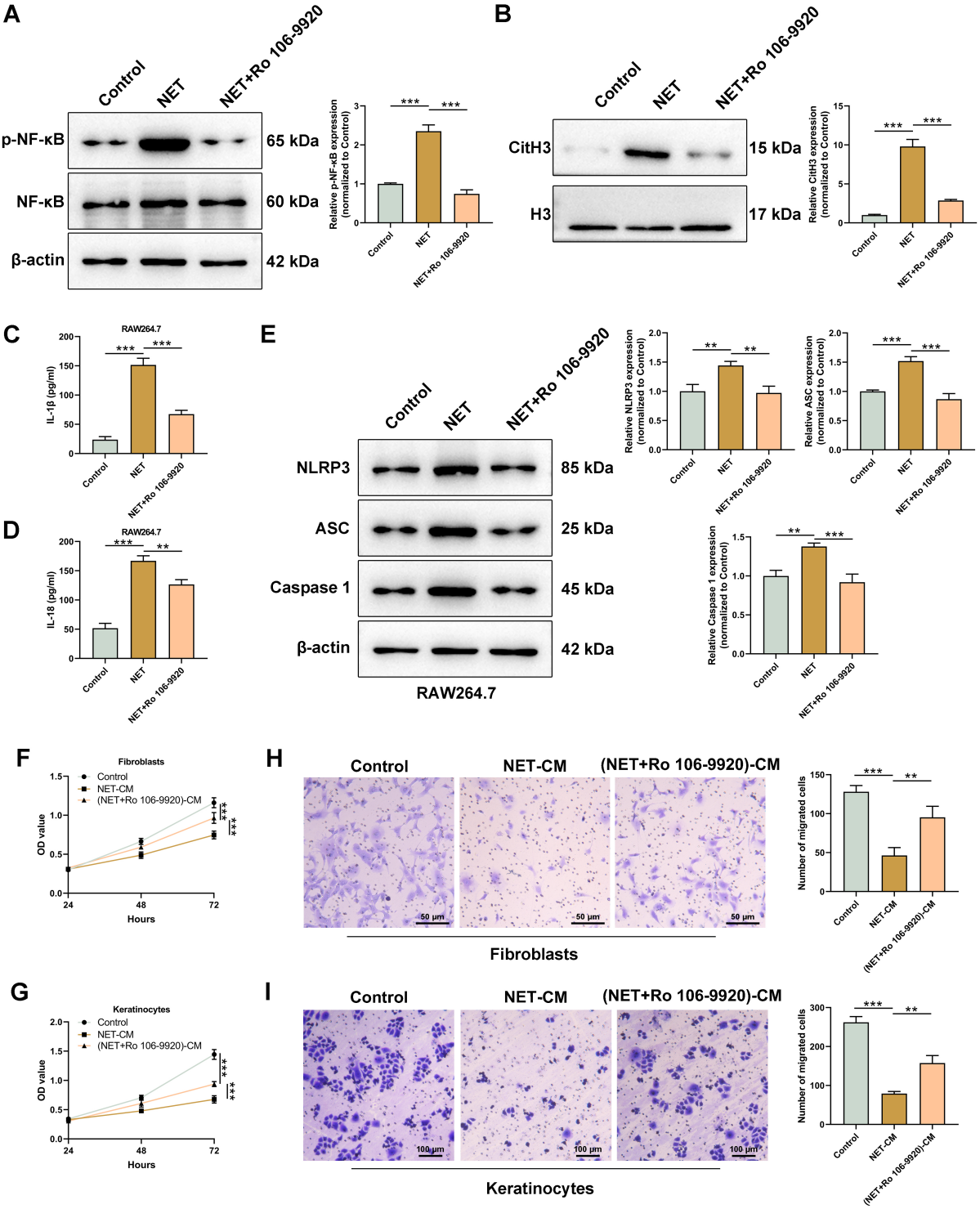

Fig. 3. Suppression of the NF-κB signaling pathway attenuates the deleterious effects of NETs on fibroblasts and keratinocytes. Mouse neutrophil-macrophage coculture models were treated with Ro 106-9920, an NF-κB inhibitor. (A) Western blot analysis verified that NF-κB activation was suppressed (n = 3 per group). (B) The relative expression of CitH3 was used as a marker of NET formation (n = 3 per group). ELISA analysis of the culture supernatant was conducted to assess the levels of proinflammatory cytokines (C) IL-1β and (D) IL-18 after Ro 106-9920 treatment (n = 3 per group). (E) NLRP3 inflammasome activation was detected through the expression of NLRP3, ASC, and caspase-1 proteins via western blot analysis (n = 3 per group). The coculturing supernatant was used as conditioned media (CM), and added to fibroblasts and keratinocytes. The viability of (F) fibroblasts and (G) keratinocytes at 24, 48, and 72 h after treatment was measured using the CCK-8 assay (n = 3 per group). The migratory ability of (H) fibroblasts (scale bar = 50 μm) and (I) keratinocytes (scale bar = 100 μm) was measured using the transwell assay (n = 3 per group). $^{**}p < 0.01$, $^{***}p < 0.001$.

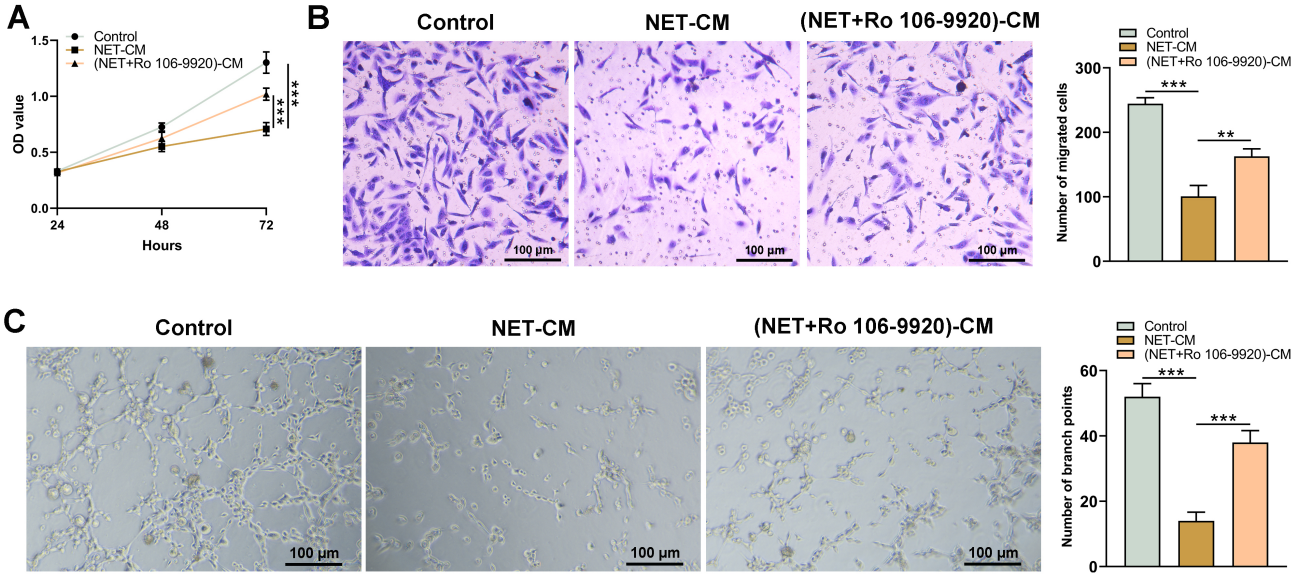

Fig. 4. Suppression of the NF-κB signaling pathway attenuates the deleterious effects of NETs on endothelial cells. CM collected from neutrophil-macrophage cocultures with or without Ro 106-9920 treatment was applied to endothelial cells for 72 h. (A) Endothelial cell viability was determined via the CCK-8 assay after 24, 48, and 72 h treatment (n = 3 per group). (B) The migration rate was evaluated using the transwell system (n = 3 per group, scale bar = 100 μm). (C) The number of branch points was calculated to analyze the angiogenic potential of endothelial cells (n = 3 per group, scale bar = 100 μm). $^{**}p < 0.01$, $^{***}p < 0.001$.

3.5 Ro 106-9920 Enhances Cutaneous Wound Healing and Re-epithelialization in DM Mice

To confirm the potential of Ro 106-9920 in promoting wound healing, we conducted an *in vivo* experiment using the diabetic mouse model (Fig. 5A). We performed subcutaneous injection of Ro 106-9920 or DMSO (vehicle) on multiple sites around the wounds of diabetic mice and monitored the dorsal wounds for 14 d. We observed a decrease in the wound area over time, with the DM+Ro 106-9920 group exhibiting significantly faster wound healing than the vehicle-treated group (Fig. 5B) ($F(3, 40) = 53.93$, $p < 0.001$). The histological evaluation further corroborated these findings. The wound area in the DM+vehicle group displayed wider and more irregular scarring with evident dermal disruption, leading to increased scar width. In contrast, the DM+Ro 106-9920 group demonstrated narrower scars with a more organized tissue architecture, indicating enhanced wound healing and re-epithelialization (Fig. 5C; $p < 0.05$). We conducted immunohistochemistry analysis for CD31 to assess angiogenesis in the wound tissues. The number of loops was significantly increased in the Ro 106-9920-treated wound compared with that in the vehicle-treated wound (Fig. 5D; $p < 0.001$). This finding suggested that Ro 106-9920 not only accelerates wound closure but also promotes angiogenesis, which is critical for effective wound healing. Notably, Ro 106-9920 treatment had no effect on the blood glucose levels and weight of DM mice (**Supplementary Fig. 2A,B**), suggesting that its beneficial role in diabetic wound healing may be independent of its antihyperglycemic effects.

3.6 Ro 106-9920 Suppresses NET Formation and NLRP3 Inflammasome Activation in Skin Wounds of DM Mice

To further elucidate the mechanism by which Ro 106-9920 enhances wound healing in DM, we assessed the levels of key proteins involved in NET formation and inflammasome activation in the wound tissues of DM mice. Treatment with Ro 106-9920 markedly reduced the expression of CitH3 and PAD4 in wound tissues (Fig. 6A). Furthermore, we observed a marked reduction in the protein levels of NLRP3 and IL-1β/pro-IL-1β in the Ro 106-9920-treated group compared with that in the Ro 106-9920-untreated control (Fig. 6B). Collectively, these findings suggested that Ro 106-9920 may accelerate wound healing in DM mice by suppressing NET formation and blocking NLRP3 inflammasome activation.

Finally, to observe whether Ro 106-9920 causes hepato- or nephro-toxicity, we conducted renal and liver biochemical and pathological evaluations during wound healing in diabetic mice. HE staining revealed no necrosis or injury in the liver sections of mice across all groups (**Supplementary Fig. 3A**). We also observed no changes in the serum ALT and AST levels across all groups of mice (**Supplementary Fig. 3B,C**). HE staining of kidneys showed an integrated architectural structure of healthy glomerular, with no necrosis in tubular cells (**Supplementary Fig. 3D**). This suggested that Ro 106-9920 has no nephrotoxicity during wound healing in diabetic mice, which was further corroborated through the evaluation of Cre and BUN levels (**Supplementary Fig. 3E,F**).

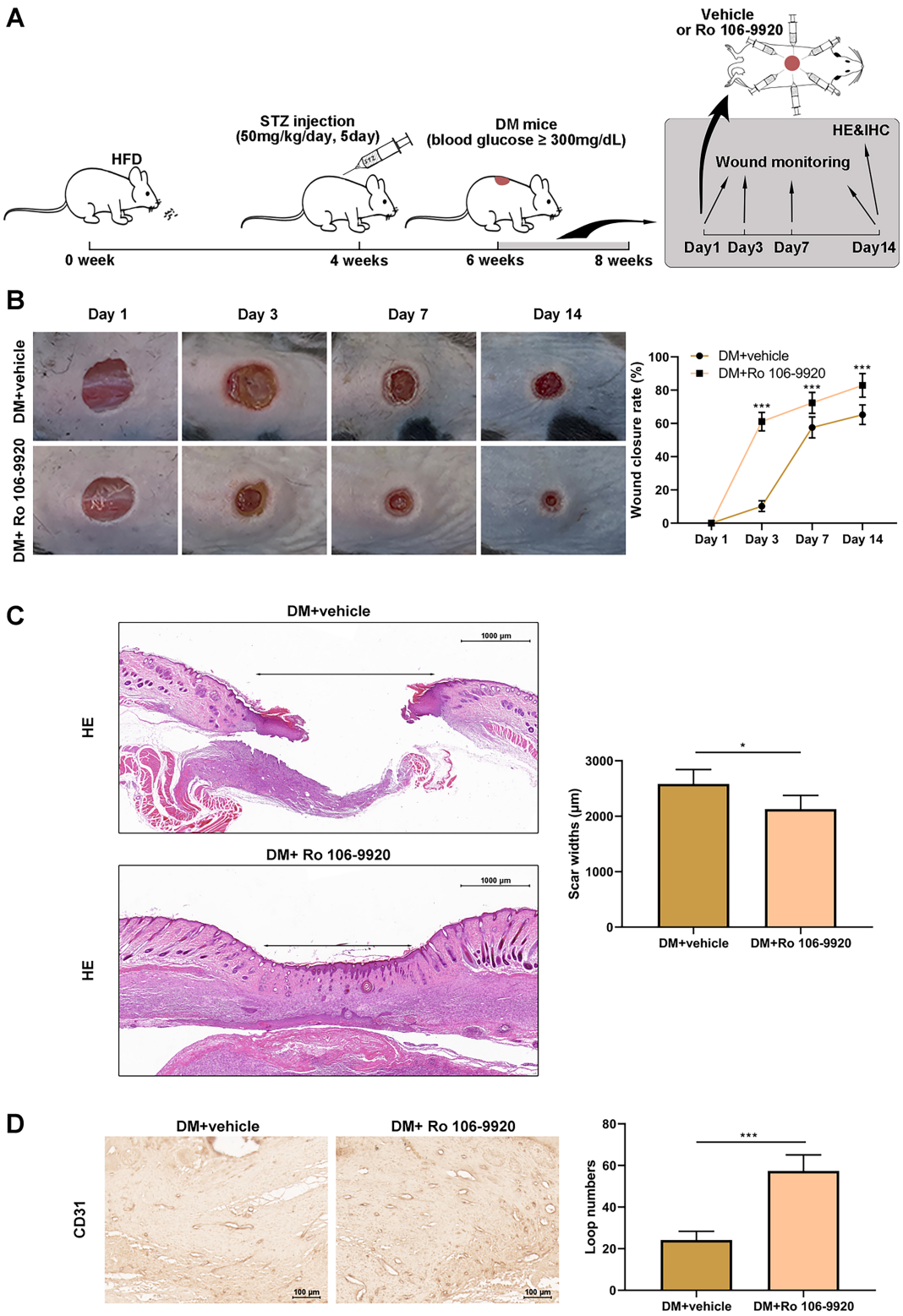

Fig. 5. Ro 106-9920 accelerates cutaneous wound healing and promotes re-epithelialization in diabetic mice. (A) Diabetic mice were subcutaneously injected with Ro 106-9920 or dimethyl sulfoxide (DMSO) (vehicle) around the wound area, and wound healing was monitored for 14 d. (B) Images of wounds on days 1, 3, 7, and 14 after wound generation, when the closure rates were also calculated (n = 3 per group). (C) Histological evaluation of wounds via hematoxylin and eosin (HE) staining. Scar width was determined using the ImageJ software (n = 3 per group). Scale bar = 1000 μm. (D) Immunohistochemical analysis of platelet endothelial cell adhesion molecule-1 (CD31) was performed to assess angiogenesis, reflected by the number of loops (n = 3 per group, scale bar = 100 μm). *$p <$ 0.05, ***$p < 0.001$. IHC, immunohistochemistry.

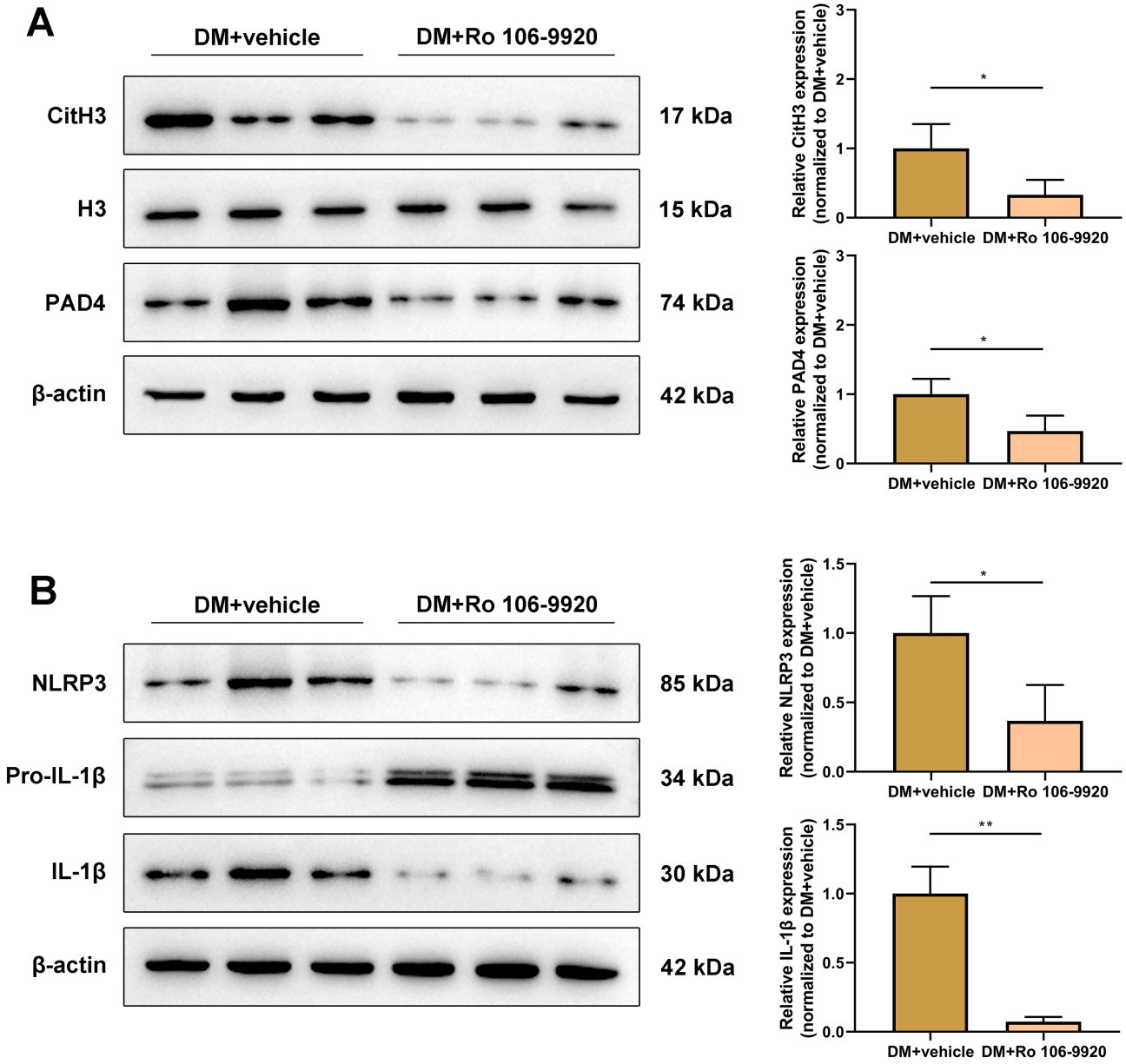

Fig. 6. Ro 106-9920 suppresses NET formation and NLRP3 inflammasome activation in the skin wounds of diabetic mice. Wound tissues of mice treated with Ro 106-9920 or DMSO were collected for western blot analysis. (A) The expression levels of CitH3 and PAD4 in wound tissues indicated NET formation (n = 3 per group). (B) NLRP3 inflammasome activation was determined by the relative protein levels of NLRP3 and IL-1β/pro-IL-1β ratios (n = 3 per group). *$p < 0.05$, **$p < 0.01$.

4. Discussion

Diabetes is a major global public health challenge, with delayed wound healing being one of its disturbing and dangerous complications [2]. Identifying potential therapeutic targets to address delayed wound healing in diabetes is crucial for the prevention and management of these complications, which have significant clinical and societal implications [1]. Herein, we investigated the potential of the NF-κB inhibitor Ro 106-9920 to enhance diabetic wound healing by suppressing NET formation and found that Ro 106-9920 promotes skin repair and angiogenesis by inhibiting NLRP3 inflammasome activation. Our results suggested that targeting NET formation is a promising strategy for improving wound healing in patients with diabetes.

During NET formation, histone H3 in neutrophils undergoes citrullination by PAD4 and is converted to CitH3, which loosens the chromatin structure and facilitates NET release [22]. However, excessive NET formation can lead to tissue damage and has been implicated in several diseases such as cardiovascular and inflammatory disorders [23]. Previous studies have demonstrated that active NET formation negatively affects wound healing, especially in some chronic inflammatory conditions including diabetes [6,24]. Herein, we observed that delayed wound healing in

diabetic mice was correlated with increased levels of CitH3 and PAD4, suggesting that heightened NET formation is a key indicator of impaired diabetic wound healing. Additionally, components of NETs, including genetic material, nuclear proteins, and pathogen-associated proteins, can act as danger-associated molecular patterns that stimulate immune cells such as macrophages. This stimulation activates the NLRP3 inflammasome, causing the maturation and release of IL-1β and IL-18 through the activation of caspase-1, which recruits more neutrophils and further enhances NET formation [25,26]. Our results demonstrated a significant and concurrent increase in NLRP3 inflammasome activation and NET formation in both the diabetic and PMA-stimulated groups compared with that in the negative controls, in consistency with this positive feedback loop. This further supports the role of NET formation and NLRP3 inflammasome activation in the pathophysiology of diabetic wounds.

Treatment with Ro 106-9920 effectively inhibited NET activation, as evidenced by a significant reduction in CitH3 levels. This was accompanied by a corresponding decrease in the expression of NLRP3 inflammasome-related proteins and release of inflammatory cytokines. Ro 106-9920 is an NF-κB-specific inhibitor, which blocks NF-κB activation by inhibiting the ubiquitination process [27], potentially suppressing NET activation through the regulation of neutrophil function and key signaling factors [28,29]. Specifically, NF-κB inhibition reduces the release of proinflammatory cytokines, alleviating the inflammatory environment and weakening neutrophil activation [30,31], indirectly inhibiting NET formation. Additionally, previous research has demonstrated that NF-κB activation promotes PAD4 expression [32,33], whereas its inhibition prevents histone citrullination, directly disrupting the initiation of NET formation [34]. Notably, although Ro 106-9920 successfully lowered IL-1β levels in diabetic wound tissues, pro-IL-1β levels were paradoxically elevated. This further confirmed the reduced NLRP3 inflammasome activation and caspase-1 release, which blocked the conversion of mature IL-1β [35], leading to the accumulation of pro-IL-1β in the tissue.

We further validated the potential of Ro 106-9920 to enhance diabetic wound healing using a series of functional assays. Fibroblasts are crucial repair cells in wound healing and are primarily responsible for synthesizing collagen and other extracellular matrix components, aiding wound contraction and tissue reconstruction [36]. Under diabetic conditions, hyperglycemia and chronic inflammation typically inhibit fibroblast migration and proliferation, preventing fibroblasts from effectively filling the wound site and slowing the healing process [37], in line with our observations.

Keratinocytes are the main cell type in the epidermis and are essential for re-epithelialization [38]. Their dysfunction is a key factor in delayed wound healing and chronic ulcer formation, which are commonly observed in patients with diabetes [39,40]. Ro 106-9920 significantly improved the viability and migration of fibroblasts and keratinocytes in the diabetic wound model-CM. This may have resulted from the mitigation in the proinflammatory environment following Ro 106-9920 treatment, as inflammation impairs fibroblast and keratinocyte function, a process closely linked to NLRP3 inflammasome activation [41,42]. Similarly, activation of the NLRP3 inflammasome induced by advanced glycation end products can promote the inflammatory infiltration of fibroblasts, thereby contributing to the development of hyperpigmentation [43]. Another study demonstrated that dampened NLRP3 inflammasome activation induced by NF-κB pathway inhibition suppressed keratinocyte proliferation and mitigated psoriasis progression [44]. Furthermore, the observed enhancement of angiogenesis in endothelial cells following Ro 106-9920 treatment, which is also critical for effective tissue regeneration, highlighted the efficacy of this compound in accelerating wound closure under diabetic conditions. This was further corroborated by the *in vivo* increase in CD31-positive vascular loops in wound tissues, a key regulator of skin wound healing in diabetic mice [45].

However, the present study had several limitations. Although our findings indicated improved wound healing in diabetic mice, the dose-response relationship, long-term effects of Ro 106-9920 on wound healing, and potential side effects were not evaluated. Further research is required to assess the chronic safety and efficacy of this treatment under diabetic conditions before it can be considered for clinical application. Additionally, although the suppression of NET formation and NLRP3 inflammasome activation were shown to enhance fibroblast, keratinocyte, and endothelial cell functions, the broader therapeutic effects of Ro 106-9920 on other cell types involved in wound healing, such as pericytes, require further investigation. A more comprehensive understanding of the means by which Ro 106-9920 influences the wound healing process across various cell types will provide greater insights into its therapeutic potential. In addition, our study also did not explore the involvement of additional pathways or biomarkers affected by NF-κB inhibition, which may provide a broader understanding of the therapeutic effect and pinpoint any off-target effects.

5. Conclusions

In summary, our findings highlighted the critical role of Ro 106-9920 in enhancing wound healing in diabetic mice by inhibiting NET formation, suggesting that targeting NETs can promote skin cell regeneration, enhance angiogenesis, and mitigate chronic inflammatory responses by blocking NLRP3 inflammasome activation in diabetic wounds. These insights provide experimental support for the investigation of Ro 106-9920 or other NET inhibitors as potential therapeutic agents for chronic nonhealing wounds in patients with diabetes. To provide stronger evidence for

clinical applications and to solidify the role of Ro 106-9920 in wound healing therapies, further verification using diabetic wound models or human cells is warranted.

Abbreviations

CCK-8, Cell Counting Kit-8; CM, conditioned medium; ELISA, enzyme-linked immunosorbent assay; NETs, neutrophil extracellular traps; PMA, phorbol 12-myristate 13-acetate; ROS, reactive oxygen species; STZ, streptozotocin.

Availability of Data and Materials

The data used and analyzed during the current study is available from the corresponding author on reasonable request.

Author Contributions

HL, LHX and JYG conceived the study and designed the experiments. JYC and HJH contributed to the data collection. FTL, SXL and FDH performed the data analysis and interpreted the results. HL and LHX wrote the manuscript. JYG contributed to the critical revision of article. All authors contributed to editorial changes in the manuscript. All authors read and approved the final manuscript. All authors have participated sufficiently in the work and agreed to be accountable for all aspects of the work.

Ethics Approval and Consent to Participate

The Ethics Review Committee of the Affiliated Hospital of Youjiang Medical University for Nationalities approved all of the experiments involving animals (YYFY-LL-2023-084). The study is reported by ARRIVE guidelines. All methods were performed following the relevant guidelines and regulations.

Acknowledgment

Not applicable.

Funding

This research received no external funding.

Conflict of Interest

The authors declare no conflict of interest.

Supplementary Material

Supplementary material associated with this article can be found, in the online version, at https://doi.org/10.31083/FBL37393.

References

[1] Matoori S. Diabetes and its Complications. ACS Pharmacology & Translational Science. 2022; 5: 513–515. https://doi.org/10.1021/acsptsci.2c00122.

[2] Burgess JL, Wyant WA, Abdo Abujamra B, Kirsner RS, Jozic I. Diabetic Wound-Healing Science. Medicina (Kaunas, Lithuania). 2021; 57: 1072. https://doi.org/10.3390/medicina57101072.

[3] Wang Z, Wei D, Li S, Tang Q, Lu G, Gu S, *et al*. Healing mechanism of diabetic foot ulcers using single-cell RNA-sequencing. Annals of Translational Medicine. 2023; 11: 210. https://doi.org/10.21037/atm-23-240.

[4] Poli V, Zanoni I. Neutrophil intrinsic and extrinsic regulation of NETosis in health and disease. Trends in Microbiology. 2023; 31: 280–293. https://doi.org/10.1016/j.tim.2022.10.002.

[5] Huang W, Jiao J, Liu J, Huang M, Hu Y, Ran W, *et al*. MFG-E8 accelerates wound healing in diabetes by regulating "NLRP3 inflammasome-neutrophil extracellular traps" axis. Cell Death Discovery. 2020; 6: 84. https://doi.org/10.1038/s41420-020-00318-7.

[6] Zhu S, Yu Y, Ren Y, Xu L, Wang H, Ling X, *et al*. The emerging roles of neutrophil extracellular traps in wound healing. Cell Death & Disease. 2021; 12: 984. https://doi.org/10.1038/s41419-021-04294-3.

[7] Rui S, Dai L, Zhang X, He M, Xu F, Wu W, *et al*. Exosomal miRNA-26b-5p from PRP suppresses NETs by targeting MMP-8 to promote diabetic wound healing. Journal of Controlled Release: Official Journal of the Controlled Release Society. 2024; 372: 221–233. https://doi.org/10.1016/j.jconrel.2024.06.050.

[8] Zhu B, Zhang X, Sun S, Fu Y, Xie L, Ai P. NF-κB and neutrophil extracellular traps cooperate to promote breast cancer progression and metastasis. Experimental Cell Research. 2021; 405: 112707. https://doi.org/10.1016/j.yexcr.2021.112707.

[9] Rosazza T, Warner J, Sollberger G. NET formation - mechanisms and how they relate to other cell death pathways. The FEBS Journal. 2021; 288: 3334–3350. https://doi.org/10.1111/febs.15589.

[10] Lian S, Li S, Zhu J, Xia Y, Do Jung Y. Nicotine stimulates IL-8 expression via ROS/NF-κB and ROS/MAPK/AP-1 axis in human gastric cancer cells. Toxicology. 2022; 466: 153062. https://doi.org/10.1016/j.tox.2021.153062.

[11] Yang L, Liu L, Zhang R, Hong J, Wang Y, Wang J, *et al*. IL-8 mediates a positive loop connecting increased neutrophil extracellular traps (NETs) and colorectal cancer liver metastasis. Journal of Cancer. 2020; 11: 4384–4396. https://doi.org/10.7150/jca.44215.

[12] Azzouz D, Khan MA, Palaniyar N. ROS induces NETosis by oxidizing DNA and initiating DNA repair. Cell Death Discovery. 2021; 7: 113. https://doi.org/10.1038/s41420-021-00491-3.

[13] Damien P, Cognasse F, Payrastre B, Spinelli SL, Blumberg N, Arthaud CA, *et al*. NF-κB Links TLR2 and PAR1 to Soluble Immunomodulator Factor Secretion in Human Platelets. Frontiers in Immunology. 2017; 8: 85. https://doi.org/10.3389/fimmu.2017.00085.

[14] Hsieh KY, Wei CK, Wu CC. YC-1 Prevents Tumor-Associated Tissue Factor Expression and Procoagulant Activity in Hypoxic Conditions by Inhibiting p38/NF-κB Signaling Pathway. International Journal of Molecular Sciences. 2019; 20: 244. https://doi.org/10.3390/ijms20020244.

[15] Ouyang L, Qiu D, Fu X, Wu A, Yang P, Yang Z, *et al*. Overexpressing HPGDS in adipose-derived mesenchymal stem cells reduces inflammatory state and improves wound healing in type 2 diabetic mice. Stem Cell Research & Therapy. 2022; 13: 395. https://doi.org/10.1186/s13287-022-03082-w.

[16] Lapponi MJ, Carestia A, Landoni VI, Rivadeneyra L, Etulain J, Negrotto S, *et al*. Regulation of neutrophil extracellular trap formation by anti-inflammatory drugs. The Journal of Pharmacology and Experimental Therapeutics. 2013; 345: 430–437. https://doi.org/10.1124/jpet.112.202879.

[17] Wishart AL, Swamydas M, Lionakis MS. Isolation of Mouse Neutrophils. Current Protocols. 2023; 3: e879. https://doi.org/10.1002/cpz1.879.
[18] Justus CR, Leffler N, Ruiz-Echevarria M, Yang LV. In vitro cell migration and invasion assays. Journal of Visualized Experiments: JoVE. 2014; 51046. https://doi.org/10.3791/51046.
[19] Xu C, Bentinger M, Savu O, Moshfegh A, Sunkari V, Dallner G, *et al*. Mono-epoxy-tocotrienol-α enhances wound healing in diabetic mice and stimulates in vitro angiogenesis and cell migration. Journal of Diabetes and its Complications. 2017; 31: 4–12. https://doi.org/10.1016/j.jdiacomp.2016.10.010.
[20] Mantovani A, Dinarello CA, Molgora M, Garlanda C. Interleukin-1 and Related Cytokines in the Regulation of Inflammation and Immunity. Immunity. 2019; 50: 778–795. https://doi.org/10.1016/j.immuni.2019.03.012.
[21] Veith AP, Henderson K, Spencer A, Sligar AD, Baker AB. Therapeutic strategies for enhancing angiogenesis in wound healing. Advanced Drug Delivery Reviews. 2019; 146: 97–125. https://doi.org/10.1016/j.addr.2018.09.010.
[22] Liu X, Li T, Chen H, Yuan L, Ao H. Role and intervention of PAD4 in NETs in acute respiratory distress syndrome. Respiratory Research. 2024; 25: 63. https://doi.org/10.1186/s12931-024-02676-7.
[23] Klopf J, Brostjan C, Eilenberg W, Neumayer C. Neutrophil Extracellular Traps and Their Implications in Cardiovascular and Inflammatory Disease. International Journal of Molecular Sciences. 2021; 22: 559. https://doi.org/10.3390/ijms22020559.
[24] Yang S, Gu Z, Lu C, Zhang T, Guo X, Xue G, *et al*. Neutrophil Extracellular Traps Are Markers of Wound Healing Impairment in Patients with Diabetic Foot Ulcers Treated in a Multidisciplinary Setting. Advances in Wound Care. 2020; 9: 16–27. https://doi.org/10.1089/wound.2019.0943.
[25] Liu D, Yang P, Gao M, Yu T, Shi Y, Zhang M, *et al*. NLRP3 activation induced by neutrophil extracellular traps sustains inflammatory response in the diabetic wound. Clinical Science (London, England: 1979). 2019; 133: 565–582. https://doi.org/10.1042/CS20180600.
[26] Singh P, Kumar N, Singh M, Kaur M, Singh G, Narang A, *et al*. Neutrophil Extracellular Traps and NLRP3 Inflammasome: A Disturbing Duo in Atherosclerosis, Inflammation and Atherothrombosis. Vaccines. 2023; 11: 261. https://doi.org/10.3390/vaccines11020261.
[27] Morinelli TA, Lee MH, Kendall RT, Luttrell LM, Walker LP, Ullian ME. Angiotensin II activates NF-κB through AT1A receptor recruitment of β-arrestin in cultured rat vascular smooth muscle cells. American Journal of Physiology. Cell Physiology. 2013; 304: C1176–C1186. https://doi.org/10.1152/ajpcell.00235.2012.
[28] An Z, Li J, Yu J, Wang X, Gao H, Zhang W, *et al*. Neutrophil extracellular traps induced by IL-8 aggravate atherosclerosis via activation NF-κB signaling in macrophages. Cell Cycle (Georgetown, Tex.). 2019; 18: 2928–2938. https://doi.org/10.1080/15384101.2019.1662678.
[29] Ai Z, Udalova IA. Transcriptional regulation of neutrophil differentiation and function during inflammation. Journal of Leukocyte Biology. 2020; 107: 419–430. https://doi.org/10.1002/JLB.1RU1219-504RR.
[30] Wright HL, Chikura B, Bucknall RC, Moots RJ, Edwards SW. Changes in expression of membrane TNF, NF-kappaB activation and neutrophil apoptosis during active and resolved inflammation. Annals of the Rheumatic Diseases. 2011; 70: 537–543. https://doi.org/10.1136/ard.2010.138065.
[31] Hayden MS, Ghosh S. NF-κB in immunobiology. Cell Research. 2011; 21: 223–244. https://doi.org/10.1038/cr.2011.13.
[32] Zeng M, Xu M, Li X, Li J, Liu Y. PAD4 silencing inhibits inflammation whilst promoting trophoblast cell invasion and migration by inactivating the NEMO/NF-κB pathway. Experimental and Therapeutic Medicine. 2022; 24: 568. https://doi.org/10.3892/etm.2022.11505.
[33] Li J, Tang RS, Shi Z, Li JQ. Nuclear factor-κB in rheumatoid arthritis. International Journal of Rheumatic Diseases. 2020; 23: 1627–1635. https://doi.org/10.1111/1756-185X.13958.
[34] Zhu D, Zhang Y, Wang S. Histone citrullination: a new target for tumors. Molecular Cancer. 2021; 20: 90. https://doi.org/10.1186/s12943-021-01373-z.
[35] Gao Y, Tu D, Yang R, Chu CH, Hong JS, Gao HM. Through Reducing ROS Production, IL-10 Suppresses Caspase-1-Dependent IL-1β Maturation, thereby Preventing Chronic Neuroinflammation and Neurodegeneration. International Journal of Molecular Sciences. 2020; 21: 465. https://doi.org/10.3390/ijms21020465.
[36] Plikus MV, Wang X, Sinha S, Forte E, Thompson SM, Herzog EL, *et al*. Fibroblasts: Origins, definitions, and functions in health and disease. Cell. 2021; 184: 3852–3872. https://doi.org/10.1016/j.cell.2021.06.024.
[37] Liu Y, Liu Y, He W, Mu X, Wu X, Deng J, *et al*. Fibroblasts: Immunomodulatory factors in refractory diabetic wound healing. Frontiers in Immunology. 2022; 13: 918223. https://doi.org/10.3389/fimmu.2022.918223.
[38] Muñoz M, Vásquez B, del Sol M. Molecular mechanisms in the process of re-epithelization in wound healing and the action of honey in keratinocytes. International Journal of Morphology. 2020; 38: 1700–1706. http://dx.doi.org/10.4067/S0717-95022020000601700.
[39] Piipponen M, Li D, Landén NX. The Immune Functions of Keratinocytes in Skin Wound Healing. International Journal of Molecular Sciences. 2020; 21: 8790. https://doi.org/10.3390/ijms21228790.
[40] Fang WC, Lan CCE. The Epidermal Keratinocyte as a Therapeutic Target for Management of Diabetic Wounds. International Journal of Molecular Sciences. 2023; 24: 4290. https://doi.org/10.3390/ijms24054290.
[41] Fenini G, Karakaya T, Hennig P, Di Filippo M, Slaufova M, Beer HD. NLRP1 Inflammasome Activation in Keratinocytes: Increasing Evidence of Important Roles in Inflammatory Skin Diseases and Immunity. The Journal of Investigative Dermatology. 2022; 142: 2313–2322. https://doi.org/10.1016/j.jid.2022.04.004.
[42] Artlett CM. The Mechanism and Regulation of the NLRP3 Inflammasome during Fibrosis. Biomolecules. 2022; 12: 634. https://doi.org/10.3390/biom12050634.
[43] Fang J, Ouyang M, Qu Y, Wang M, Huang X, Lan J, *et al*. Advanced Glycation End Products Promote Melanogenesis by Activating NLRP3 Inflammasome in Human Dermal Fibroblasts. The Journal of Investigative Dermatology. 2022; 142: 2591–2602.e8. https://doi.org/10.1016/j.jid.2022.03.025.
[44] Li J, Yan W, Ren F, Sang H. Tectorigenin inhibits inflammation in keratinocytes by inhibition of NLRP3 inflammasome regulated by the TLR4/NF-κB pathway. Allergologia et Immunopathologia. 2023; 51: 82–89. https://doi.org/10.15586/aei.v51i2.780.
[45] Icli B, Nabzdyk CS, Lujan-Hernandez J, Cahill M, Auster ME, Wara AKM, *et al*. Regulation of impaired angiogenesis in diabetic dermal wound healing by microRNA-26a. Journal of Molecular and Cellular Cardiology. 2016; 91: 151–159. https://doi.org/10.1016/j.yjmcc.2016.01.007.